KGML-ag: A Modeling Framework of Knowledge-Guided Machine Learning to Simulate Agroecosystems: A Case Study of Estimating N₂O Emission using Data from Mesocosm Experiments

Licheng Liu[1], Shaoming Xu[2], Jinyun Tang[3], Kaiyu Guan[4,5,6], Timothy J. Griffis[7], Matthew D. Erickson[7], Alexander L. Frie[7], Xiaowei Jia[8], Taegon Kim[1, 9], Lee T. Miller[7], Bin Peng[4,5,6], Shaowei Wu[10], Yufeng Yang[1], Wang Zhou[4,5], Vipin Kumar[2], Zhenong Jin[1,11]*

[1]Department of Bioproducts and Biosystems Engineering, University of Minnesota, Saint Paul, MN, 55108, USA
[2]Department of Computer Science and Engineering, University of Minnesota, Minneapolis, MN, 55455, USA
[3]Climate and Ecosystem Sciences Division, Lawrence Berkeley National Laboratory, Berkeley, CA 94720, USA
[4]Agroecosystem Sustainability Center, Institute for Sustainability, Energy, and Environment, University of Illinois at Urbana-Champaign, Urbana, IL 61801, USA
[5]Department of Natural Resources and Environmental Sciences, University of Illinois at Urbana-Champaign, Urbana, IL 61801, USA
[6]National Center for Supercomputing Applications, University of Illinois at Urbana-Champaign, Urbana, IL 61801, USA
[7]Department of Soil, Water, and Climate, University of Minnesota, Saint Paul, MN 55108, USA
[8]Department of Computer Science, University of Pittsburgh, Pittsburgh, PA, 15260, USA
[9]Department of Smart Farm, Jeonbuk National University, Jeonju, Jeollabuk-do, 54896, Republic of Korea
[10]School of Physics and Astronomy, University of Minnesota, Minneapolis, MN, 55455, USA
[11]Institute on the Environment, University of Minnesota, Saint Paul, MN, 55108, USA

Correspondence to: Zhenong Jin (jinzn@umn.edu)

Abstract.

Agricultural nitrous oxide (N₂O) emission accounts for a non-trivial fraction of global greenhouse gases (GHGs) budget. To date, estimating N₂O fluxes from cropland remains a challenging task because the related microbial processes (e.g., nitrification and denitrification) are controlled by complex interactions among climate, soil, plant and human activities. Existing approaches such as process-based (PB) models have well-known limitations due to insufficient representations of the processes or uncertainties of model parameters, and to leverage recent advances in machine learning (ML) a new method is needed to unlock the "black box" to overcome its limitations such as low interpretability, out-of-sample failure and massive data demand. In this study, we developed a first-of-kind knowledge-guided machine learning model for agroecosystems (KGML-ag), by incorporating biogeophysical/chemical domain knowledge from an advanced PB model, *ecosys*, and tested it by comparing simulating daily N₂O fluxes with real observed data from mesocosm experiments. The Gated Recurrent Unit (GRU) was used as the basis to build the model structure. To optimize the model performance, we have investigated a range of ideas, including: 1) Using initial values of intermediate variables (IMVs) instead of time series as model input to reduce data demand; 2) Building hierarchical structures to explicitly estimate IMVs for further N₂O prediction; 3) Using multitask learning to balance the simultaneous training on multiple variables; and 4) Pretraining with millions of synthetic data generated from *ecosys* and fine tuning with mesocosm observations. Six other pure ML models were developed using the same mesocosm data to serve as the benchmark for the KGML-ag model. Results show that KGML-ag did an excellent job in reproducing the mesocosm

N$_2$O fluxes (overall r^2 = 0.81, and RMSE = 3.6 mg N m^{-2} day^{-1} from cross-validation). Importantly KGML-ag always outperforms the PB model and ML models in predicting N$_2$O fluxes, especially for complex temporal dynamics and emission peaks. Besides, KGML-ag goes beyond the pure ML models by providing more interpretable predictions as well as pinpointing desired new knowledge and data to further empower the current KGML-ag. We believe the KGML-ag development in this study will stimulate a new body of research on interpretable ML for biogeochemistry and other related geoscience processes.

1 Introduction

Nitrous oxide (N$_2$O), with its global warming potential 273 $\pm$ 118 times greater than that of carbon dioxide (CO$_2$) for a 100-year time horizon, is one of the major greenhouse gases (IPCC6; Forster et al., 2021). The increasing rate of atmospheric N$_2$O concentration during the period 2010-2015 is 44% higher than during 2000-2005, mainly driven by increased anthropogenic sources that have increased total global N$_2$O emissions to ~17 Tg N yr^{-1} (Syakila and Kroeze, 2011; Thompson et al., 2019). It is estimated that approximately 60% of the contemporary N$_2$O emission increases are from agriculture management at global scale (Pachauri et al., 2014; Robertson et al., 2014; Tian et al., 2020), but the estimation uncertainty can exceed 300% (Barton et al., 2015; Solazzo et al., 2021). Quantifying N$_2$O emissions from agricultural soils is extremely challenging, partly because the related microbial processes, mainly about incomplete denitrification and nitrification, are controlled by many environment and management factors such as temperature/water conditions, soil/crop properties, and N fertilization rate, all of which together have collectively led to large temporal and spatial variabilities of N$_2$O emissions (Butterbach-Bahl et al., 2013; Grant et al., 2016).

Process-based (PB) models are often used for simulating N$_2$O fluxes from agroecosystems, but they have some inherent limitations, including incomplete knowledge of the processes, low accuracy due to the under-constrained parameters, expensive computing cost, and rigid structure for further improvements, that we could not resolve by using PB model itself. For example, an advanced agroecosystem model, *ecosys* (Grant et al., 2003, 2006, 2016), simulates N$_2$O production rates through nitrification and denitrification processes when oxygen (O$_2$) is limited, with equations considering the influence from related substrate concentrations (e.g., NO$_2^-$, N$_2$O, and CO$_2$), nitrifier and denitrifier populations, and soil thermal, hydrological physical and chemical conditions. The produced N$_2$O accumulates, transfers in gaseous phase, aqueous phase, over different soil layers, and eventually exchanges with atmosphere at the soil surface. Other PB models, including DNDC (Zhang et al., 2002; Zhang and Niu, 2016), DAYCENT (Del Grosso et al., 2000; Necpálová et al., 2015), and APSIM (Keating et al., 2003; Holzworth et al., 2014), have also included processes to simulate N$_2$O production, but adopt different parameterizations using static partition parameters to estimate N$_2$O emission from nitrification, and other empirical parameters to control the influence on nitrification from soil water content, pH, temperature and substrate concentrations. Besides, N$_2$O is intimately connected with the soil organic carbon (SOC) dynamics, because soil nitrifiers and denitrifiers interact strongly with aerobic and anaerobic heterotrophs that process SOC evolution, and all of these microbes are driven by shared environmental variables

including soil temperature, moisture, redox status, and physical and chemical properties (Thornley et al., 2007). As expected, these connections make it difficult for PB models, even the most advanced ones like *ecosys*, to find sufficient representations of the physical and biogeochemical processes or obtain enough data to calibrate a large number of model parameters with strong spatio-temporal variations. Thus, novel approaches are needed for addressing the big challenge of agricultural N_2O flux simulations.

Machine learning (ML) models can automatically learn patterns and relationships from data. Recent studies have investigated the potential to predict agricultural N_2O emission with ML models, including random forest (RF, Saha et al., 2021), metamodelling with extreme gradient boosting (XGBoost) (Kim et al., 2021), and deep learning neural network (DNN) (Hamrani et al., 2020). Notably, Hamrani et al. (2020) compared nine widely used ML models for predicting agricultural N_2O. That study pointed out that the long short term memory (LSTM) model with recurrent networks containing memory cells as building blocks will be most suitable for N_2O predictions, but the challenge remains with respect to the ability of capturing the sharp peak of N_2O fluxes and lag time between N fertilizer application and the emission peak. Although there is an increasing interest in leveraging recent advances in machine learning, capturing this opportunity requires going beyond the ML limitations, including limited generalizability to out-of-sample scenarios, demand for massive training data, and low interpretability due to the "black-box" use of ML (Karpatne et al., 2017). PB models with their transparent structures built by representations of physical and biogeochemical processes, seem to be exact complementary to ML models. Thus, combining the power of ML model and PB model understanding innovatively is likely a path forward.

The above need to integrate ML and PB models can be potentially addressed by the newly proposed framework of Knowledge-guided Machine Learning (KGML) models. In the review by Willard et al. (2021), five research frontiers have been identified regarding the development of KGML for diverse disciplines including earth system science, they are: 1) Loss function design according to physical or chemical laws (Jia et al., 2019, 2021; Read et al., 2019); 2) Knowledge-guided initialization through pretraining ML models with synthetic data generated from PB models (Jia et al., 2019, 2021; Read et al., 2019); 3) Architecture design according to causal relations or adding dense layers containing domain knowledge (Khandelwal et al., 2020; Beucler et al., 2019, 2021); 4) Residual modeling with ML models to reduce the bias between PB model outputs and observations (Hanson et al., 2020); and 5) Other hybrid modeling approaches combining PB and ML models (Kraft et al., 2021). These recent advances in KGML pave the pathway to a more efficient, accurate and interpretable solution for estimating N_2O fluxes from the agroecosystem.

In this study, we present a first-of-its-kind attempt of developing a KGML for agricultural GHG fluxes prediction (KGML-ag) with knowledge-guided initialization and architecture design, and demonstrate the potential of KGML-ag with a case study on quantifying N_2O flux observed by a multi-year mesocosm experiments. We designed the KGML-ag structure based on the causal relations of related N_2O processes informed by an advanced agroecosystem model, *ecosys* (Grant et al., 2003, 2006,

2016). We used the synthetic data generated from *ecosys* to design the KGML-ag input/output, and to pre-train the KGML-ag model to learn the basic patterns of each variable. Observations from multi-season controlled-environment mesocosm chambers (Miller, 2021, thesis; Miller et al., 2021, in review) were used to refine the pretrained KGML-ag and evaluate the model performance. Since there is limited literature that guides the development of KGML-ag and not a one that directly addressed GHG fluxes, we investigated a range of ideas to optimize the model performance, including: 1) Using initial values of intermediate variables (IMVs) instead of sequences as model input to reduce data demand; 2) Building hierarchical structures to explicitly estimate IMVs for further N_2O prediction; 3) Using multitask learning to balance the simultaneous training on multiple variables; and 4) Pretraining with millions of synthetic data generated from *ecosys* and fine tuning with mesocosm observations. Although we evaluated the KGML-ag models with real measurements only from a mesocosm experiment, the lessons learned from the development process and various KGML-ag structures can be transferred to other data, other variables and large scale simulations, therefore have broader implications on further KGML related research in agriculture. We believe this study will stimulate a new body of research on interpretable machine learning for biogeochemistry and other related topics in geoscience.

2 Methods

2.1 Experimental design overview

To develop and evaluate the KGML-ag models and compare their performance with pure ML models, we designed the following experiments:

1) With the synthetic data, we developed and pretrained multiple KGML-ag models to learn general patterns and interactions among variables, and evaluated their model performance (Fig. S2, Table 1);

2) With the observed data, we finetuned multiple KGML-ag models to adapt real-world situations, and evaluated their model performance (Fig. 2-3; Fig. S3-5; Table 2-3);

3) We further benchmarked KGML-ag models and uncertainties with other pure ML models without considering temporal dependence, including Decision Tree (DT), Random Forest (RF), Gradient Boosting (GB) from the sklearn package (https://scikit-learn.org/stable/), Extreme Gradient Boosting (XGB) from the XGBoost package (https://xgboost.readthedocs.io/en/latest/) and a 6-linear-layer artificial neural network (ANN) with the mesocosm experiment data by 10 times ensemble experiments (Fig. 4-5; Fig. S6-8);

4) We conducted a few small experiments to further investigate how various model configurations, such as the pretraining process, data augmentation and IMV initial values would influence KGML-ag model performance (Table 3).

2.2 KGML-ag structure development

2.2.1 Generating synthetic data with *ecosys*

We generated synthetic data using a PB model, *ecosys*. The *ecosys* model is an advanced agroecosystem model constructed from detailed biophysical and biogeochemical rules instead of using empirical relations (Grant et al., 2001). It represents N_2O evolution in the microbe-engaged processes of nitrification-denitrification using substrate kinetics that are sensitive to soil nitrogen availability, soil temperature, soil moisture, and soil oxygen status (Grant and Pattey 2008). Two groups of microbial populations, autotrophic nitrifiers and heterotrophic denitrifiers, produce N_2O with specific competitive or cooperative relations in *ecosys* when O_2 availability fails to meet O_2 demand for their respirations and NO_2^- become alternative electron acceptors. N_2O transfer within soil layers and from soil to the atmosphere is driven by concentration gradient using diffusion-convection-dispersion equations, in the forms of gaseous and aqueous N_2O under control of volatilization-dissolution (Grant et al., 2016). Unlike the pipeline model described by Davidson et al. (2000) , which mainly consider the correlations of N_2O production with nitrogen availability and of N_2O emissions with soil water content, *ecosys* enables integrative effects of energy, water, nitrogen availability on N_2O production and N_2O transfer via the microbial population dynamics and their interactions with soil, plant, and atmospheric dynamics, under diverse meteorological and anthropogenic disturbances (e.g. runoff, drainage, tillage, irrigation, soil erosion). Many previous studies have demonstrated its robustness in simulating agricultural carbon and nitrogen cyclings at different spatial/temporal scales, and under different management practices (Grant et al., 2003, 2006, 2016; Metivier et al., 2009; Zhou et al., 2021). For the agricultural ecosystems in the US Midwest, whose simulations are used for synthetic data in this study, the performance of *ecosys* on CO_2 and N_2O fluxes have been extensively benchmarked, including CO_2 exchange (NEE, $R^2 = 0.87$) and leaf area index (LAI, $R^2 = 0.78$) from six flux towers, USDA census reported corn yield ($R^2 = 0.83$) and soybean yield ($R^2 = 0.80$), satellite-derived GPP for corn ($R^2 = 0.83$) and soybean ($R^2 = 0.85$) from Illinois, Iowa and Indiana, and cumulative N_2O emissions ($R^2 = 0.36$) across eight Midwestern states (Wang et al., 2021; Yang et al., 2022). Therefore, *ecosys* is an appropriate choice of domain knowledge provider and synthetic data generator in the development of KGML models. We generated daily synthetic data including N_2O flux and 76 IMVs (e.g. CO_2 flux from soil, layerwise soil NO_3^- concentration, layerwise soil temperature, and layerwise soil moisture; detailed in Table S1) from *ecosys* simulations for 2000-2018 over 99 randomly selected counties in Iowa, Illinois, and Indiana, USA. We used hourly meteorological inputs (downward shortwave radiation, air temperature, precipitation, relative humidity, and wind speed) from the phase 2 of North American Land Data Assimilation System (NLDAS-2, Xia et al., 2012) and layerwise soil properties (e.g. bulk density, texture, pH, SOC concentration) from the SSURGO database (Soil Survey Staff, 2020) as inputs to *ecosys*. Crop management except N fertilization rates were configured to the same settings as mesocosm experiments (described in Sec 2.2.2). To increase the variability in synthetic data, we implemented 20 different N fertilization rates ranging from 0 to 33.6 g N m^{-2} (i.e. 0 to 300 lb N ac^{-1}) in each simulation of 99 counties, and more detailed information for model setup refers to Zhou et al. (2021).

The generated synthetic data were then processed for further use by KGML-ag development. Meanwhile, the hourly weather forcings were converted to seven daily variables, including the maximum air temperature (TMAX_AIR, $^\circ$C), difference between the maximum and the minimum air temperature (TDIF_AIR, $^\circ$C), the maximum humidity (HMAX_AIR, fraction), difference between the maximum and the minimum humidity (HDIF_AIR, fraction), surface downward shortwave radiation (RADN, W m^{-2}), precipitation (PREC, mm day^{-1}), and wind speed (WIND, m s^{-1}). Six soil properties were retrieved from the SSURGO database, including total averaged (depth weighted averaged for all layers) bulk density (TBKDS, Mg m^{-3}), sand content (TCSAND, g kg^{-1}), silt content (TCSILT, g kg^{-1}), pH (TPH), cation exchange capacity (TCEC, cmol$^+$ kg^{-1}) and soil organic carbon (TSOC, g C kg^{-1}); and two crop properties were retrieved, including planting day of the year (PDOY) and crop type (CROPT, 1 for corn and 0 for soybean). Finally, each synthetic data sample has daily N$_2$O flux, 76 selected IMVs, 7 weather forcings (W), 1 N fertilization rate (FN, g N m^{-2}) and 8 soil/crop properties (SCP) (Fig. 1.a; Table S1). The periods from April 1st to July 31st (122 days) were selected to cover the mesocosm observations (around 30 days before and 90 days after N fertilizer date). The total amount of synthetic data sample is 122 days x 18 years x 99 counties x 20 N fertilizer rates (about 4.3 million data points). We randomly selected the samples from 70 counties for training, 10 counties for validation, and 19 counties for testing.

2.2.2 Mesocosm experiments for KGML-ag model fine-tuning and evaluation

Observations were acquired from a controlled-environment mesocosm facility on the St. Paul campus of the University of Minnesota. Soil samples were sourced in 2015 from a farm in Goodhue County, MN (44.2339° N and 92.8976° W), which had been under corn-soybean rotation for 25 years. Six chambers with a soil surface area of 2 m^2 and column depth of 1.1 m were used to plant continuous corn during 2015-2018 and monitor the N$_2$O flux response to different precipitation treatments. The experiment also measured other environmental variables including air temperature and photosynthetically active radiation (PAR), which were controlled to mimic the outdoor ambient environment. Granular urea fertilizer was hand broadcasted and incorporated to a depth of 0.05 m to each chamber at a rate of 22.4 g N m^{-2} (200 lb N ac^{-1}) on May 1st of 2015, May 4th of 2016 and May 3rd of 2017, and 10.3 g N m^{-2} (92 lb N ac^{-1}) on May 8th of 2018. Corn hybrid (DKC-53-56RIB) were hand planted to a depth of 0.05 m in two rows spaced 0.76 m apart 3-5 days after fertilizer application, at a seeding rate of 35,000 seeds ac^{-1} in 2015 to 2017, and 70,000 seeds ac^{-1} in 2018 but thinned upon emergence to ensure 100 percent emergence at 35,000 seeds ac^{-1}. Crops were harvested at the end of September by cutting the stover five inches above the soil. Hourly N$_2$O fluxes (mg N m^{-2} h^{-1}) and CO$_2$ fluxes (g C m^{-2} h^{-1}) were measured using non-steady-state flux chambers with a CO$_2$ analyzer (LI-10820 for 2016 and LI-7000 for 2017 and 2018, LI-COR Biosciences, Lincoln, NE) and a N$_2$O analyzer (Teledyne M320EU, Teledyne Technologies International Corp, Thousand Oaks, CA) (Detail method can be retrieved from Fassbinder et al., 2012, 2013). We also collected soil moisture at 15 cm depth (VWC as abbreviation of volumetric water content, m^3 m^{-3}), weekly 0-15 cm depth soil NO$_3^-$ + NO$_2^-$ concentration (NO$_3^-$ for short in the following text, g N Mg^{-1}), soil NH$_4^+$ concentration (NH$_4^+$, g N Mg^{-1}), and related environment variables including air temperature, radiation, humidity and soil/crop

198   properties from three growing seasons during 2016-2018 and six mesocosm chambers (Fig. S1). The magnitude of N_2O flux

199   and NO_3^- soil concentration and their responses following fertilizer application from this mesocosm experiment are consistent

200   with several field studies of agricultural soils (Fassbinder et al., 2013; Grant et al., 1999, 2006, 2008; Hamrani et al., 2020;

201   Venterea et al., 2011) More details about the mesocosm facility and experimental design can be found in the thesis of Miller

202   L. (2021).

203

204   The observed data were then processed to fine-tune and evaluate the KGML-ag models. The N_2O flux and four IMVs and

205   weather variables were collected from the measurements in the selected period (i.e., April 1st to July 31st). Weekly NO_3^- (short

206   for soil NO_3^- within 0-15 cm depth), and NH_4^+ (short for soil NH_4^+ within 0-15 cm) were linearly interpolated to the daily time

207   scale on days containing VWC (short for soil VWC in 15 cm) data. Hourly air temperature, net radiation, N_2O (short for N_2O

208   fluxes from soil), CO_2 (short for CO_2 fluxes from soil) and VWC were resampled to daily scale. All SCP were derived from

209   mesocosm measurements except that TCEC was derived from the SSURGO database according to the soil origin. We used the

210   leave-one-out cross-validation (LOOCV) method for the finetuning and evaluation process. Each time we used one chamber

211   data for validation and another five chambers' data for model finetuning.

212

213   To reduce overfitting and increase the generalization of the trained model based on the small amount of mesocosm data, we

214   applied the following method to augment the experimental measurements and weather forcings to 1000 times larger by

215   sampling hourly data and averaging them to daily scale. In this method, 16 hours (or maximum valid hours) of data are

216   randomly selected from 24 hours of data to compute their mean as the daily value. Since 3/4 of the day are covered by the

217   selected data (16 hours /24 hours), the augmented daily values should be representative enough for the source day and

218   meanwhile present slight variations. Furthermore, the observation ratio, (24 hours - missing hours) / 24 hours, can be used as

219   the weights in loss function to inject the data quality information in model optimization. If the day has more than 16 hours

220   missing values, we consider the observations in that day as not trustworthy and drop the day by setting the weight to 0. This

221   method can not only augment the data to 1000 times larger but also deal with the missing values in observed data inherently.

222   The total amount of observed mesocosm data and related weather forcings are augmented to 122 days x 3 years x 6 chambers

223   x 1000 data samples in this study.

224

225   **2.2.3 Gated Recurrent Unit (GRU) as the basis of KGML-ag**

226   Hamrani et al. (2020) compared different models and reported that LSTM provided the highest accuracy in predicting N_2O

227   fluxes, because N_2O flux is time dependent by its production/consumption nature and LSTM simulates target variables by

228   considering both current and historical states. The LSTM model, proposed by Hochreiter and Schmidhuber (1997), uses a cell

229   state as an internal memory to preserve the historical information. At each time step, it creates a set of gating variables to filter

230   the input and historical information and then uses the processed data to update the cell state. Similar to LSTM, GRU is a gated

recurrent neural network but only keeps one hidden state (Cho et al., 2014). Though simpler than LSTM, GRU is proved to have similar performance (Chung et al., 2014). Our preliminary test on synthetic data for N_2O prediction showed that GRU indeed provided similar or higher accuracy and model efficiency under different model settings than LSTM (Table S2). This is possible because simpler models with fewer weights and hyperparameters are more robust in combating the overfitting problem. Therefore, we choose GRU as the basis of KGML-ag development.

2.2.4 Incorporating domain knowledge to the development of KGML-ag

To quantitatively reveal the correlations between N_2O fluxes and IMVs and guide the KGML-ag development, we conducted feature importance analysis by a customized 4-layer GRU ML model (Fig. 1b). Each layer of the model has a GRU cell with 64 hidden units. The 4-layer structure makes the model deeper and capable of capturing complex interactions. Between each GRU cell, 20% of the output hidden states are randomly dropped by replacing them with zero values (so called 20% dropout) to avoid overfitting. A linear dense layer is used to map the final output to N_2O. We first trained GRU models using synthetic data with different combinations of IMVs as inputs to predict the N_2O fluxes (original-test, Table S2). The feature importance analysis of well-trained models was then implemented by replacing one input feature with a Gaussian noise with mean $\mu=0$ and standard deviation $\sigma=0.01$, while keeping others untouched (new-test). The importance score was calculated by the new-test's root mean square error (RMSE) (replacing one feature) minus the original-test's RMSE (no replacing). RMSE was calculated by $\frac{\sqrt{\Sigma_1^N (y_i - y_i')^2}}{N}$ where N is the total number of observations across time and space, y_i is i-th measurement from synthetic data or observed data and y_i' is its corresponding prediction.

To find important variables for N_2O flux prediction in an ideal situation where all variables are available, we conducted a feature importance analysis for GRU models with all IMVs and basic inputs including FN, 7 W and 8 SCP (Fig. S2a). Results indicated that flux variables including NH_3, H_2, N_2, O_2, CH_4, evapotranspiration (ET) and CO_2 had significant influence on the model performance. Variables ranked high in feature importance analysis are considered with priority during model development. To develop a functionable KGML-ag, we further investigated the feature importance of four IMVs that are available from mesocosm observations including CO_2, NO_3^-, VWC and NH_4^+, which were ranked 7th, 20th, 58th, 60th respectively in 92 input features of synthetic data (Fig. S2a). We used these four available IMVs to create two input combinations: 1) CO_2 flux, NO_3^-, VWC and NH_4^+ (IMVcb1), and 2) NO_3^-, VWC and NH_4^+ (IMVcb2). The objective of building IMVcb2 was to investigate the importance of highly ranked variable CO_2 flux (by removing it from the inputs), and the impact of mixing-up flux and non-flux variables on model performance. We tested the feature importance of the GRU models built with IMVcb1 and IMVcb2 to check whether they would help in N_2O prediction (Fig. S2b-c). All the feature importance results above indicated the correlation intensity between N_2O and many other variables, which would help the KGML-ag model development and interpretation in this study (rest of this section and Sec. 3.1), and would guide future N_2O related measurements and KGML model development (discussed in Sec. 4.3).

263

264   Next we used the knowledge learned from synthetic data to develop the structure of KGML-ag (Fig. 1c-d). Previous studies

265   for KGML models have used physical laws, e.g., conservation of mass or energy, to design the loss function for constraining

266   the ML model to produce physically consistent results (Read et al., 2019; Khandelwal et al., 2020). However, for complex

267   systems like agroecosystems, it is challenging to incorporate physical laws, such as mass balance for N_2O, into the loss function

268   due to the incomplete understanding of the processes and the lack of mass balance related data for validation. An alternative

269   solution is to incorporate such information in the design of the neural network (Willard et al., 2021). Effectiveness of such an

270   approach was demonstrated by Khandelwal et al. (2020) in the context of modeling stream flow in a river basin using Soil &

271   Water Assessment Tool (SWAT). They used a hierarchical neural network to explicitly model IMVs (e.g., soil moisture, snow

272   cover) and their relationships with the target variable (streamflow) and showed that this model is much more effective than a

273   neural network that attempts to directly learn the relationship between input drivers and the target variables. Following this

274   idea, we identified four desired features of an effective KGML-ag model, including: 1) We used initial values instead of

275   sequence of the IMVs from synthetic data or observed data to provide a solid starting state for the ML system and reduce the

276   IMV data demand, and then used the rest of the data to further constrain the prediction of IMVs; 2) We built a hierarchical

277   structure based on the structure of process representation in *ecosys* to first predict IMVs and then simulate N_2O with predicted

278   IMVs; 3) We trained all variables together using multitask learning to reach the best prediction scores, which generalized the

279   model and incorporated interactions between IMVs and N_2O; 4) We initialized the KGML-ag model by pretraining with

280   synthetic data before using real observed data to transfer physical knowledge, which further reduced the demand on large

281   training samples and aided in faster convergence for fine-tuning.

282

283   To meet these desired features, we proposed two KGML-ag models (Fig. 1c-d). The first model, KGML-ag1, is a hierarchical

284   structure containing two modules to simulate IMVs and N_2O sequentially. Each module is a 2-layer 64 units GRU ML model.

285   The inputs to the module of the KGML-ag1 model for IMV predictions (KGML-ag1-IMV module) are FN, 7W and 8SCP

286   together with the initial values of IMVs, and the outputs are IMV predictions. The inputs to the module of the KGML-ag1

287   model for N_2O predictions (KGML-ag1-N_2O module) are FN, 7W, 8SCP and predicted IMVs from KGML-ag1-IMV, and the

288   output is the target variable N_2O. Linear dense layers were coded for both modules to map output states to IMVs or N_2O. The

289   dropout method was applied to drop 20% of the state output between GRU cells and dense layers. The second model, KGML-

290   ag2, is also a hierarchical structure similar to KGML-ag1, but has multiple KGML-ag2-IMV modules to explicitly simulate

291   IMVs by tuning them separately in the fine-tuning process (discussed in Sec. 2.2.5). Each KGML-ag2-IMV module in KGML-

292   ag2 is a 2-layer 64 units GRU cell with the inputs of FN+7W+8SCP and one IMV initial value, and the output of one IMV

293   prediction. The KGML-ag2-N_2O module collects the IMV predictions from KGML-ag2-IMV modules and predicts the N_2O

294   with inputs of FN+7W+8SCP and predicted IMVs.

2.2.5 Strategies for pretraining and fine-tuning processes

To increase the efficiency of the training process, we used the Z-normalization ($\frac{(X-\mu)}{\sigma}$, where X is the vector of a particular variable over all the data samples in the data set; μ is the mean value of X; σ is the standard deviation of X) method to normalize each variable separately on synthetic data. Then the scaling factors (μ, σ) derived from *ecosys* synthetic data for each variable were used to Z-normalize observed data into the same ranges as synthetic data. As mentioned in Sec. 2.2.1, the TDIF_AIR, HDIF_AIR were used instead of absolute min temperature (TMIN_AIR) and humidity (HMIN_AIR). This is done because TMIN_AIR and HMIN_AIR follow similar trends as TMAX_AIR and HMAX_AIR, making Z-normalization numerically poorly defined. Using the difference between maximum and minimum can provide a clearer information of daily air temperature/humidity variation.

During the pretraining process, we initialized the IMV of KGML-ag using the first day value of synthetic IMV time series. Adam optimizer with a start learning rate of 0.0001 was used for the training process. The learning rate would decay by 0.5 times after every 600 training epochs. At each epoch, synthetic data samples were randomly shuffled before being input to the model to predict N_2O (and IMVs if any). The mean square error (MSE) loss (calculation was equal to the square of RMSE) or sum of MSE loss (if multitask learning) between predictions and *ecosys* synthetic observations were calculated to optimize the weights of GRU cells. After the training process updated the model's weights, the validation process was performed to evaluate the model performance based on untouched samples with RMSE and the square of Pearson correlation coefficient (r^2). r^2 was calculated as $\frac{(\Sigma_i\ (y_{i'}-\underline{y_{i'}})(y_i-\underline{y_i}))^2}{\Sigma_i\ (y_{i'}-\underline{y_{i'}})^2(y_i-\underline{y_i})^2}$, where y_i is the i-th measurement from synthetic data or observed data, y_i' is its corresponding prediction, $\underline{y_i}$ is the mean of the measurement y in diagnosing space and $\underline{y_i}'$ is the mean of the predicted y' in diagnosing space. If both validated r^2 and RMSE were better than the best values in previous epochs, the updated model in this epoch would be saved. Normalized RMSE (NRMSE, calculated by RMSE/(max-min) of each variable observation) was introduced to evaluate IMV predictions between variables with different value ranges.

During the fine-tuning process, we used estimated IMV initial values of 1.0 g C m^{-2}, 0.2 m^3 m^{-3}, 0.0 g N Mg^{-1}, and 20.0 g N Mg^{-1} for CO_2, VWC, NH_4^+, and NO_3^- respectively, from starting day (April 1st) to the day before the first day of real observations, as input to KGML-ag models. Then the first-day values of observed IMVs were input into KGML-ag during the rest days of the period as IMV initial values. In addition, as described in Sec. 2.2.2, we used a data augmentation method to augment the total amount of data 1000 times larger for the fine-tuning process. The purpose of this data augmentation method was to increase the generalization of the fine-tuned model and to overcome the overfitting due to small sample size. The mask matrix was elementarily multiplied to the output matrix to calculate the MSE, r^2 and RMSE only for days with observations. The similar optimizer was used with an initial learning rate of 0.00005 and decay fraction of 0.5 per 200 epochs. Other training/validation methods in each epoch were similar to the pretraining process. Specifically, in the KGML-ag1 model

finetuning process, we first froze the KGML-ag1-N$_2$O module and only trained the KGML-ag1-IMV module for IMVs. After finishing the KGML-ag1-IMV module training, we froze the KGML-ag1-IMV module and trained the KGML-ag1-N$_2$O module for N$_2$O. In the KGML-ag2 fine-tuning process, the similar freezing method was used but different KGML-ag2-IMV modules were trained separately one by one.

2.3 Development environment description

We used the Pytorch 1.6.0 (https://pytorch.org/get-started/previous-versions/) and python 3.7.9 (https://www.python.org/downloads/release/python-379/) as the programing environment for the model development. In order to use the GPU to speed-up the training process, we installed cudatoolkit 10.2.89 (https://developer.nvidia.com/cuda-toolkit). A desktop with Nvidia 2080 super GPU was used for code development and testing. The Mangi cluster (https://www.msi.umn.edu/mangi) from High Performance Computing of Minnesota Supercomputing Institute (HPC-MSI, https://www.msi.umn.edu/content/hpc) with 2-way Nvidia Tesla V100 GPU was used in training processes which consumed longer time and bigger memories.

3 Results

3.1 Pretraining experiments using synthetic data from *ecosys*

In the pretraining stage, the GRU model with 76 IMVs achieved the best performance in predicting N$_2$O fluxes (r^2=0.98, RMSE =0.54 mg N m^{-2} day^{-1} and normalized RMSE (NRMSE) = 0.01) on the test set of synthetic data generated from *ecosys* (Table 1). The high performance was due to some flux IMVs such as NH$_3$, H$_2$, O$_2$, CO$_2$ and ET, which are highly correlated to N$_2$O (Fig. S2a), were used as input to the model. The good performance of GRU with all IMVs indicates that ML models are able to perfectly mimic *ecosys* when sufficient information about IMVs is available. The GRU model with only basic input of N fertilizer rate, 7 weather forcings, and 8 soil/crop properties (FN+7W+8SCP) had the accuracy of r^2=0.89 and RMSE = 1.37 mg N m^{-2} day^{-1} (Table 1). The relatively low performance is likely because this model failed to capture several highly nonlinear pathways that are employed by ecosys to predict N$_2$O (e.g., one influence pathway from precipitation to N$_2$O can be: Precipitation → soil moisture → N components solubility/concentration → nitrification/denitrification rate/amount → soil N$_2$O concentration → gas N$_2$O flux). When adding sequences of IMV combinations (i.e., IMVcb1 of CO$_2$ flux, NO$_3^-$, NH$_4^+$ and VWC, and IMVcb2 of NO$_3^-$, NH$_4^+$ and VWC), the GRU models performed slightly better than the GRU model using only basic inputs, achieving r^2 of 0.92 and 0.90, respectively (Table 1). The KGML-ag1 with IMVcb1 and IMVcb2 initial values provided better performance (both r^2 = 0.90) than GRU with basic input and comparable performance to the GRU with inputs of IMVcb1 and IMVcb2 sequence. Besides, KGML-ag1 provided predicted IMVs of CO$_2$, NO$_3^-$, NH$_4^+$, and VWC with r^2 over 0.91, and NRMSE below 0.06 (Table 1). KGML-ag2 also provided comparable N$_2$O performance but relatively better IMVs

356 performance of r^2 over 0.92 and NRMSE below 0.05. Results indicated that KGML-ag models with IMV initial values as extra
357 input performed similar or better than pure ML models in synthetic data.

3.2 KGML-ag evaluation using observed data from mesocosm

359 After being fine-tuned with observed data, KGML-ag1 had N$_2$O prediction overall accuracy of r^2=0.81 and RMSE=3.6 mg N
360 m^{-2} day^{-1}, while non-pretrained GRU model provided r^2=0.78 and RMSE=4.0 mg N m^{-2} day^{-1}, and pretrained GRU model
361 provided r^2=0.80 and RMSE=3.77 mg N m^{-2} day^{-1} (Table 3). The time series of N$_2$O predictions from KGML-ag1 and the non-
362 pretrained GRU model were further compared (Fig. 2), from which we found at least two advantages of using KGML-ag1 for
363 N$_2$O predictions: 1) For the region without observation data (normally before day 25), KGML-ag1 predicted stable N$_2$O fluxes
364 close to 0 mg N m^{-2} day^{-1} (which is close to the reality in the experiment setting) while GRU caused anomalous peaks of fluxes.
365 This is because KGML-ag1 has learned knowledge for the whole period from the pretraining process with *ecosys* model
366 generated synthetic data, but GRU model has no prior knowledge for the period without any data in observations; 2) Although
367 KGML-ag1 had a lower accuracy than GRU in some chambers, KGML-ag1 can better capture the temporal dynamics of N$_2$O
368 fluxes compare to GRU, especially when the fluxes are highly variable (e.g. Fig 2 chamber 2).

370 To validate KGML-ag1 robustness, we further investigated the KGML-ag1 and GRU model performance in different temporal
371 windows, shrinking from the whole period to the N$_2$O peak occurrence time (days 1-122, day 30-80, day 40-65 and day 45-60
372 for year 2016-2018), and performance in N$_2$O flux, first order gradient of N$_2$O (slope) and second order gradient of the N$_2$O
373 (curvature) (Table 2). Slope represents the speed of N$_2$O flux changes through time and curvature represents the acceleration.
374 Assessing prediction performance with these two metrics will reveal the model robustness on capture variable dynamics, which
375 is critical when predicting fast-change variables with hot moments like N$_2$O. First of all, the overall r^2 and RMSE of KGML-
376 ag1 for values, slope and curvature were always better than GRU. In particular, KGML-ag1 captured the peak region (e.g.,
377 days 45-60) much better than GRU in both magnitude and dynamics (Table 2, Fig 2). Even for chamber 2 and 5 in
378 which KGML-ag1 made worse N$_2$O predictions than GRU (Δr^2 ranging from -0.07 to -0.03), it better captured temporal
379 dynamics than GRU in terms of slope (Δr^2 ranging from 0.08 to 0.16) and curvature (Δr^2 from 011 to 0.23) (Table 2). For other
380 chambers, KGML-ag1 outperformed GRU consistently. For chamber 1, KGML-ag1 had worse N$_2$O predictions RMSE than
381 GRU but the Δr^2 increased as the window shrinks to the peak emission time (0.07 → 0.13). The slope and curvature for
382 chamber 1 also indicated that KGML-ag1 captured the dynamics much better than GRU. For chamber 3, KGML-ag1 predicted
383 better N$_2$O but presented worse slope and curvature RMSE than GRU (Table 2). However, when explicitly investigating the
384 time series of N$_2$O flux, slope and curvature in each year, KGML-ag1 outperformed GRU more significantly in 2017, the year
385 with more complex temporal dynamics of N$_2$O fluxes, than in 2016 and 2018, especially for chamber 3 (Fig. 2; Fig. S3-4).
386 This investigation supported that KGML-ag1 was more capable for complex dynamics predictions.

Interestingly, the fine-tuned KGML-ag1 model predicted reasonable IMVs including CO_2, NO_3^-, NH_4^+, and VWC with overall r^2 of 0.37, 0.39, 0.60, and 0.33 and NRMSE of 0.14, 0.21, 0.09 and 0.18, respectively (Table 3). The time series comparisons between IMV predictions and observations further indicated that KGML-ag1 could reasonably capture both magnitude and dynamics (Fig. 3). KGML-ag2 presented better IMVs predictions than KGML-ag1, with overall r^2 of CO_2, NO_3^-, NH_4^+, and VWC increasing by 0.37, 0.17, 0.06 and 0.51, and NRMSE decreasing by 0.05, 0.03, 0.01 and 0.10, respectively, but a slightly lower r^2 (decreasing 0.02) of N_2O (Table 3; Fig. S5). This indicated that explicitly simulating each IMV with separated KGML-ag2-IMV modules did not benefit the N_2O flux prediction accuracy, likely due to increasing model complexity which resulted in reduced stability and ignoring the IMV interactions. In addition, we also found all KGML-ag models would perform better by using IMVcb1 (with CO_2) than using IMVcb2 (without CO_2) in real data tests, indicating feature importance analysis based on synthetic data can be a reasonable substitute for analysis with the often limited real-world data.

3.3 KGML-ag comparing with other pure ML models

The results from eight different models showed that KGML-ag1 comparing with other pure ML models consistently provided the lowest RMSE (3.59-3.94 mg N m^{-2} day^{-1}, 1.14-1.23 mg N m^{-2} day^{-2}, and 0.84-0.89 mg N m^{-2} day^{-3}) and highest r^2 (0.78-0.81, 0.48-0.56, and 0.23-0.31) for N_2O fluxes, slope and curvature, respectively (Fig. 4). This indicated that KGML-ag1 outperformed other pure ML models in capturing both the magnitude and dynamics of N_2O flux. KGML-ag2 presented slightly better mean scores for N_2O flux predictions than KGML-ag1, but worse scores for slope and curvature and larger uncertainties. This proved the hypothesis discussed in section 3.2 that KGML-ag2 didn't benefit the magnitude and dynamics predictions of N_2O flux with its more complex structure and less connections between IMVs.

Within the tree-based models (DT, RF, GB and XGB), the simplest model DT provided the worst predictions for N_2O flux, slope and curvature. The XGB model provided the highest N_2O flux accuracy with r^2 of 0.61-0.63 and RMSE of 5.07-5.17 mg N m^{-2} day^{-1}, while the GB model provided best slope and curvature predictions with r^2 of 0.38-0.40 and 0.23-0.26, and RMSE of 1.34-1.37 mg N m^{-2} day^{-2} and 0.91-0.95 mg N m^{-2} day^{-3}, respectively. The highest N_2O flux accuracy and relatively low slope and curvature accuracy of the XGB model implied that there is a trade-off between the abilities of capturing dynamics and magnitude.

In the group of deep learning models including ANN, GRU and KGML-ag1, ANN provided the worst predictions. Even with the better N_2O flux predictions than most tree-based models (except XGB), the slope and curvature predictions of ANN were the worst among all eight models. This implied that the trade-off between accurately capturing N_2O dynamics to magnitude in ANN was significant. But when considering the temporal dependence, deep learning model GRU and KGML-ag1 outperformed all other models in flux, slope and curvature predictions. This indicated that without considering temporal dependence the improvement in N_2O flux prediction accuracy could be risky by causing the performance drop in capturing dynamics.

421

The detailed model comparisons in each chamber are shown in Fig. 5 (N_2O flux) and Fig. S6-7 (N_2O slope and curvature), where the results are found to follow the same pattern as described above. In addition, time series comparisons of chamber 3 and 4 in 2017 between different models are presented in Fig. S8 as two examples. From these comparisons, we infer that without considering temporal dependence and pretraining process, the tree-based model including DT, RF, GB and XGB and deep learning model ANN predicted erratic peaks in almost every missing data point, while GRU model was stable in small gaps and only presented poor performance in long missing period (before 25 day). This improvement by GRU model can be attributed to the structure of GRU that naturally keeps the historical information using hidden states, which enables GRU to consider the temporal dependence and make consistent predictions over time.

3.4 Influence of pretraining process, data augmentation and using IMV initial values as input feature

After we pretrained the GRU model with synthetic data, the overall r^2 of N_2O flux predictions in observed data increased by 0.02, 0.12 and 0.14, and RMSE decreased by 0.23 mg N m^{-2} day^{-1}, 0.15 mg N m^{-2} day^{-2} and 0.02 mg N m^{-2} day^{-3} for flux, slope and curvature predictions, respectively, compared to non-pretrained GRU (Table 3 gray region). The gap between the GRU model with pretrain and KGML-ag1 in N_2O value prediction shows the improvement resulting from architecture change (r^2 increases by 0.01 and RMSE decreases by 0.17 mg N m^{-2} day^{-1}). Although pretrained GRU had higher slope and curvature prediction accuracy than KGML-ag models, it still couldn't achieve the current N_2O value prediction accuracy of KGML-ag1. Besides, the KGML-ag models had relatively shallow N_2O prediction modules (2-layer GRU KGML-ag-N_2O module of KGML-ag models vs 4-layer GRU) but included modules for IMV predictions, which therefore increased the model interpretability.

It's worth noting that prediction accuracy of all KGML-ag models dropped without augmenting the training dataset in the fine-tuning process (Table 3 blue region). Moreover, the maximum training epochs increased from 800 to 20000, which resulted in overfitting on the small data set. This indicated that the data augmentation indeed helped the models become more generalizable and gain better accuracy.

Experiments using zero initial values presented a significant drop in every variable's prediction accuracy (Table 3 yellow region). This indicated that the IMV initial values input into the KGML-ag-IMV modules of KGML-ag models influenced not only the IMV prediction but also the N_2O prediction of the KGML-ag-N_2O module. This shows that there is useful information transferred from IMVs in the KGML-ag-IMV module to the KGML-ag-N_2O module.

4 Discussion

In the previous section, we showed that KGML-ag models can outperform ML models, by invoking architectural constraints and PB model synthetic data initialization. Compared to traditional PB models such as *ecosys*, KGML-ag models provide computationally more accurate and efficient predictions (KGML-ag few seconds vs *ecosys* half hour), which is similar to traditional ML surrogate models (Fig. S9). But KGML-ag goes beyond that by providing more interpretable predictions than pure ML models.

4.1 Interpretability of KGML-ag

The proposed KGML-ag models incorporate causal relations among N_2O related variables/processes as shown in Fig. S10. Managements, weather forcings and initial values of IMVs influence soil water, soil temperature and soil properties, which influence the availability of O_2 and N as well as the microbe populations in soil, and further influence the nitrification and denitrification rates. N_2O is produced during both nitrification and denitrification when soil O_2 concentration is limited. Our KGML-ag follows this hierarchical structure by designing KGML-ag-IMV modules representing the soil processes for IMVs predictions (Fig. 1c-d).

To better explain the time series predictions of N_2O flux (Fig. S1; Fig. 2-3), we separated the observations of each year into three periods: leading period (before N_2O increasing), increasing period (increasing to the peak) and decreasing period (peak decreasing to near zero). During the leading period, both NH_4^+ and CO_2 were increasing immediately in the following few days following urea N fertilizer application, indicating that urea was decomposing into NH_4^+ and CO_2 in soil water. With accumulating NH_4^+ in soil, nitrification started producing NO_3^- and consuming O_2. N_2O didn't respond to the fertilizer immediately due to enough O_2 in soil. Then when the soil became sufficiently hypoxic, N_2O fluxes entered an increasing period with N_2O being produced by nitrification and denitrification processes. CO_2 fluxes were relatively low and NH_4^+ kept decreasing during this period. Finally, when soil NH_4^+ was exhausted and NO_3^- started decreasing due to denitrification, N_2O fluxes then entered the decreasing period. CO_2 flux was related to urea decomposition during the leading period, and was more closely related to O_2 demand in other periods. The KGML-ag predictions of N_2O and IMV captured the three periods and transition points, demonstrating the connections between those variables following the description as above (Fig. 3; Fig. S5). Although KGML-ag1 obtained lower IMVs prediction accuracy compared to KGML-ag2, it captured the general trends and was doing better for transitions, especially in NH_4^+ predictions. KGML-ag2 overfitted on the observations and ignored the correlations between IMVs, which resulted in loss in pretrain knowledge, poorer performance in the leading period, and erratic predictions in the period with missing observations (before day 25).

4.2 Lessons for KGML-ag development

The development of KGML-ag in our study is suitable to predict not only N_2O but also other variables, such as CO_2, CH_4 and ET, with complicated generation processes relying on the historical states. To develop a capable KGML model, we need to carefully address three questions:

What kind of ML model is suitable for developing KGML? The answer could be determined by the dominant variation type of the target variable in the data. If the dominant type is temporal variance, like flux variables in high temporal resolution (e.g., daily, or hourly), we should consider ML models with temporal dependency. RNN models such as GRU used in this study, and CNN models such as casual CNN (Oord et al., 2016) can be good starting ML models. If the dominant type is spatial variation, like variables in coarse temporal resolution (e.g., monthly or annually) but with high diversity due to soil property, land cover and climate, we should consider ML models with the ability to deal with edges, hotpoints and categories, such as CNN;

What physical/chemical constraints can be used to build KGML models? Although physical rules such as mass balance or energy balance are conceptually straightforward and were proved capable of constraining KGML in predicting lake phosphorus and temperature dynamics (Hanson et al., 2020; Read et al., 2019), they were excluded in this study according to our preliminary analysis. The reason is that the mass balance equation of N in the agriculture ecosystem includes too many unknown and unobservable components such as N_2 flux, NH_3 flux, N leaching, microbial N, plant N and soil/plant exchange, which collectively introduce large uncertainties in balance equations and make them hard to be directly applied in the KGML-ag framework. Other related physical (e.g., diffusion, solution) or chemical (e.g., nitrification, denitrification) processes cannot be easily added into the KGML-ag structure as rules due to lack of understanding of the process. Instead, as mentioned in Sect. 2.2.4, we used hierarchical structure to enforce an architectural constraint and causal relations among variables, and pretraining processes to infuse knowledge from *ecosys* to KGML-ag models.

How to involve PB models in the KGML development? An advanced PB model like *ecosys* built upon biophysical and biochemical rules instead of empirical relations will be a good basis to learn the process, guide the structure and provide the constraints for KGML. The generated synthetic data in this study helped us get some knowledge about variables such as their general trends, dynamics and correlations. Such knowledge can be transferred to KGML models from synthetic data in the pretraining process, which can reduce the efforts to collect large numbers of real-world observation data. Moreover, while KGML shows great potential beyond PB models, we reckon that equally important for improving N_2O modeling is to continue improving our understanding of the related processes and mechanisms. Novel data collection and incorporating new understanding into PB models (e.g., *ecosys*) could provide foundation to further empower KGML (see further discussion in Sect. 4.3).

4.3 Limitation and possible improvement

First, the KGML-ag models in this study are limited by the available observed data. Some IMVs with high feature importance scores (e.g., O_2 flux, N_2 flux) or at different depths (e.g., soil NO_3^- at 5 cm depth, VWC at 5 cm depth), and data out of growing seasons are not included. The direct consequences are that some important processes cannot be well represented by the current KGML-ag (e.g., O_2 demand and N availability for nitrification and denitrification). Further improvement of KGML should consider three categories of data: target variable N_2O flux, IMVs and basic inputs (Fig. 1a). For N_2O flux observation, we lack sub-hourly to sub-daily observations to capture the hot moment of emission during 0-30 days after N fertilizer applications. Besides, the non-growing season can provide 35-65% of the annual direct N_2O emissions from seasonally frozen croplands and lead to a 17–28 % underestimate of the global agricultural N_2O budget if ignoring its contribution (Wagner-Riddle et al., 2017), but we can barely find observations from non-growing seasons. For IMVs, we found oxygen demand indicator (e.g., O_2 concentration or flux, CO_2 flux, CH_4 flux), N mass balance related variables (e.g., N_2 flux, soil NO_3^-, soil NH_4^+, N leaching) and soil water and temperature, can be used to better constrain the processes and therefore improve the KGML performance. Rohe et al. (2021) also indicated the importance of O_2, CO_2 and N_2 soil fluxes for N_2O predictions. In addition, the layerwise soil observations (e.g., soil NO_3^-, soil VWC) at 0-30 cm depth can be used to significantly improve the KGML model quality, according to our feature importance analysis (Fig. S2a). Moreover, continuous monitoring on these variables during the whole year is preferred rather than only during the growing season, since N_2O flux is largely influenced by previous states. To apply the KGML-ag to large scale, other observational data including basic inputs of soil/crop properties (e.g., soil bulk density, pH, crop type), management information (e.g., fertilizer, irrigation, tillage) and weather forcings along with N_2O flux observations are critical for fine-tuning and validating the developed KGML-ag and therefore explicitly simulating the N_2O or IMVs dynamics under specific conditions. Recent advances in remote sensing and machine learning have enabled estimating these variables with high-resolution at a large scale (Peng et al., 2020)

Second, the physical/chemical constraints can be more comprehensive in KGML-ag models. Although current KGML-ag models are well-initialized with *ecosys* synthetic data and constrained by causal relations of processes with hierarchical structure, the predicted N_2O flux and IMVs can still violate some basic physical rules like mass balance. As we discussed in Sec. 4.2, it will be challenging to add physical rules like mass balance equation for N in a complicated agriculture ecosystem due to data limitations such as missing observations on certain key variables. Using inequalities instead of equations for mass balance may be one alternative solution. For example, we could use ReLU to add in a limitation for N mass balance residues which are calculated from known terms not larger than an empirical static value. Besides, better understanding of processes in the N cycle from fieldworks and lab experiments can also help us design new constraints. This limitation is also partially related to the data limitation and can be overcomed by involving more complete N_2O data to introduce more powerful constraints to KGML-ag.

Third, the KGML-ag currently are suffering from dealing with physical/chemical boundary transitions. Boundary transitions are common in the real world, such as phase change, volume solubility, and soil porosity etc. A detailed PB model generally coded plenty of "if/else/switch" statements inside to deal with the boundaries. But KGML-ag models based on the GRU are better at capturing continuous changes, rather than discrete changes. One solution is to include data with boundary information. In this study, involving IMVs like O_2, CO_2 and N_2, which already have boundary information like water freezing point, N pool volumes and other complicated boundaries related to soil/crop properties, can significantly improve the model performance. The data with boundary information could be continuous observation or estimated value from existing data. By using initial values to predict IMVs, KGML-ag in this study can partially solve the boundary transition problem when observation data is limited. Another solution is designing new structures of KGML-ag, such as combining ReLU function or including CNN model which are robust for discrete situations to the RNN models, or designing new constraints to limit the model working within the thresholds.

Finally, at the current stage we can not claim to have completely opened the black box of KGML-ag, but this framework is a significant step towards this goal. For example, some ideas implemented in our study, such as using pretraining to transfer knowledge from PB model to ML model, incorporating causal relations by hierarchical structure, predicting IMVs for tracking middle changes and using initial values as input to reduce data demand, would shed light on the future KGML-ag framework improvement. Besides, we acknowledge the importance of further testing the KGML-ag over completely independent datasets, but results presented in this manuscript are sufficient to justify the power of KGML as a framework. The mesocosm experiment data we used in this study has provided a comprehensive set of inputs and intermediate variables in addition to the output of N_2O fluxes, thus serving as a unique testbed. We expect our validation results will be more solid once more gold standard data of N_2O fluxes along with other relevant inputs and intermediate variables become publicly available. Moreover, incorporating more and more domain knowledge into KGML-ag will be inevitable in further improvement, but we don't think KGML-ag will become inefficient as it becomes more like the PB model. In fact, to efficiently surrogate components of PB models has been proposed as a research frontier in hybrid modeling for earth system science (Reichstein et al., 2019; Irrgang et al., 2021), with latest advances occurring in weather forecasts (Bauer et al., 2021). By using a hybrid model, computationally inefficient components of PB can be identified one by one, and be replaced with more efficient ML-based surrogates to eventually obtain the most efficient model. Further KGML-ag model development will also need to balance efficiency, accuracy and interpretability.

5 Conclusions

In this study, two KGML-ag models have been developed, validated, and tested for agricultural soil N_2O flux prediction using synthetic data generated by the PB model *ecosys* and observational data from a mesocosm facility. The results show that

KGML-ag models can outperform PB and pure ML models in N_2O prediction in not only magnitude (KGML-ag1 $r^2 = 0.81$ vs best ML model GRU $r^2 = 0.78$) but also dynamics (KGML-ag1 accuracy minus GRU accuracy, slope $\Delta r^2 = 0.06$ and curvature $\Delta r^2 = 0.08$). KGML-ag can also defeat the PB model *ecosys* in efficiency by completing *ecosys*'s half-hour job within a few seconds. Compared to ML models, KGML-ag models can better represent complex dynamics and high peaks of N_2O flux. Moreover, with IMV predictions and hierarchical structures, KGML-ag models can provide biogeophysical/chemical information about key processes controlling N_2O fluxes, which will be useful for interpretable forecasting and developing mitigation strategies. Data demand for the KGML-ag models is significantly reduced due to involving IMV initial values and pretrain processes with synthetic data. This study demonstrated that the potential of KGML-ag application in the complex agriculture ecosystem is high and illustrates possible pathways of KGML-ag development for similar tasks. Further improvement of our KGML-ag models can involve general principles to further constrain the predictions through loss functions or architectures, but call for more detailed, high temporal resolution N_2O observation data from field measurements.

Code and Data Availability

The code and data used in this study can be found at https://doi.org/10.5281/zenodo.5504533.

Author contributions

LL and ZJ conceived the study. WZ and YY conducted *ecosys* simulations and provided synthetic data. LL and SX processed the data and developed the KGML-ag model. LL, SX and SW carried the experiments out with supervisions from ZJ, JT, KG, and VK. TJG, MDE, ALF and LTM shared mesocosm observations and interpreted the data. LL wrote the first draft of manuscript with further editing from TK on figure and tables. ZJ, SX, JT, KG, XJ, BP, YY, WZ and VK further edited the manuscript.

Competing interests

The authors declare that they have no conflict of interest.

References

Barton, L., Wolf, B., Rowlings, D., Scheer, C., Kiese, R., Grace, P., ... & Butterbach-Bahl, K.: Sampling frequency affects estimates of annual nitrous oxide fluxes, Scientific reports, 5(1), 1-9, 2015.

Bauer, P., Dueben, P. D., Hoefler, T., Quintino, T., Schulthess, T. C., & Wedi, N. P.: The digital revolution of Earth-system science. Nature Computational Science, 1(2), 104-113, 2021.

Beucler, T., Pritchard, M., Rasp, S., Ott, J., Baldi, P., & Gentine, P.: Enforcing analytic constraints in neural networks emulating physical systems, Physical Review Letters, 126(9), 098302, 2021.

Beucler, T., Rasp, S., Pritchard, M., & Gentine, P.: Achieving conservation of energy in neural network emulators for climate modeling, arXiv preprint arXiv:1906.06622, 2019.

Butterbach-Bahl, K., Baggs, E. M., Dannenmann, M., Kiese, R., & Zechmeister-Boltenstern, S.: Nitrous oxide emissions from soils: how well do we understand the processes and their controls? Philosophical Transactions of the Royal Society B: Biological Sciences, 368(1621), 20130122, 2013.

Cho, K., Van Merriënboer, B., Bahdanau, D., & Bengio, Y.: On the properties of neural machine translation: Encoder-decoder approaches, arXiv preprint arXiv:1409.1259, 2014.

Chung, Junyoung, Caglar Gulcehre, KyungHyun Cho, and Yoshua Bengio.: Empirical evaluation of gated recurrent neural networks on sequence modeling, arXiv preprint arXiv:1412.3555, 2014.

Daw, A., Thomas, R. Q., Carey, C. C., Read, J. S., Appling, A. P., & Karpatne, A.: Physics-guided architecture (pga) of neural networks for quantifying uncertainty in lake temperature modeling, In Proceedings of the 2020 siam international conference on data mining (pp. 532-540), Society for Industrial and Applied Mathematics, 2020.

Del Grosso, S. J., Parton, W. J., Mosier, A. R., Ojima, D. S., Kulmala, A. E., & Phongpan, S.: General model for N_2O and N2 gas emissions from soils due to dentrification, Global biogeochemical cycles, 14(4), 1045-1060, 2020.

Fassbinder, J. J., Schultz, N. M, Baker, J. M, & Griffis, T. J.: Automated, Low-Power Chamber System for Measuring Nitrous Oxide Emissions, Journal of environmental quality, 42, 606. doi: 10.2134/jeq2012.0283, 2013.

Fassbinder, J. J., Griffis, T. J., & Baker, J. M.: Evaluation of carbon isotope flux partitioning theory under simplified and controlled environmental conditions, Agricultural and forest meteorology, 153, 154-164, 2012.

Forster, P., Storelvmo, T., Armour, K. , Collins, W., … & Zhang, H.: The Earth's Energy Budget, Climate Feedbacks, and Climate Sensitivity. In: Climate Change 2021: The Physical Science Basis. Contribution of Working Group I to the Sixth Assessment Report of the Intergovernmental Panel on Climate Change, Cambridge University Press. In Press, 2021.

Gilhespy, S. L., Anthony, S., Cardenas, L., Chadwick, D., del Prado, A., Li, C., ... & Yeluripati, J. B.: First 20 years of DNDC (DeNitrification DeComposition): model evolution, Ecological modelling, 292, 51-62, 2014.

Grant, R. F.: Modeling Carbon and Nitrogen Dynamics for Soil Management, (Boca Raton, FL: CRC Press) A review of the Canadian ecosystem model ecosys 173–264, 2021.

Grant, R. F., & Pattey, E.: Modelling variability in N_2O emissions from fertilized agricultural fields, Soil Biology and Biochemistry, 35(2), 225-243, 2003.

Grant, R. F., & Pattey, E.: Temperature sensitivity of N_2O emissions from fertilized agricultural soils: Mathematical modeling in ecosys. Global biogeochemical cycles, 22(4), 2008.

Grant, R. F., Neftel, A., & Calanca, P.: Ecological controls on N_2O emission in surface litter and near-surface soil of a managed grassland: modelling and measurements, Biogeosciences, 13(12), 3549-3571, 2016.

Grant, R. F., Pattey, E., Goddard, T. W., Kryzanowski, L. M., & Puurveen, H.: Modeling the effects of fertilizer application rate on nitrous oxide emissions, Soil Science Society of America Journal, 70(1), 235-248, 2006.

Hamrani, A., Akbarzadeh, A., & Madramootoo, C. A.: Machine learning for predicting greenhouse gas emissions from agricultural soils, Science of The Total Environment, 741, 140338, 2020.

Hanson, P. C., Stillman, A. B., Jia, X., Karpatne, A., Dugan, H. A., Carey, C. C., ... & Kumar, V.: Predicting lake surface water phosphorus dynamics using process-guided machine learning, Ecological Modelling, 430, 109136, 2020.

Holzworth, D. P., Huth, N. I., deVoil, P. G., Zurcher, E. J., Herrmann, N. I., McLean, G., ... & Keating, B. A.: APSIM–evolution towards a new generation of agricultural systems simulation, Environmental Modelling & Software, 62, 327-350, 2014.

Irrgang, C., Boers, N., Sonnewald, M., Barnes, E. A., Kadow, C., Staneva, J., & Saynisch-Wagner, J.: Towards neural Earth system modelling by integrating artificial intelligence in Earth system science. Nature Machine Intelligence, 3(8), 667-674, 2021.

Jia, X., Willard, J., Karpatne, A., Read, J. S., Zwart, J. A., Steinbach, M., & Kumar, V.: Physics-guided machine learning for scientific discovery: An application in simulating lake temperature profiles, ACM/IMS Transactions on Data Science, 2(3), 1-26, 2021.

Jia, X., Willard, J., Karpatne, A., Read, J., Zwart, J., Steinbach, M., & Kumar, V.: Physics guided RNNs for modeling dynamical systems: A case study in simulating lake temperature profiles, In Proceedings of the 2019 SIAM International Conference on Data Mining (pp. 558-566), Society for Industrial and Applied Mathematics, 2019.

Karpatne, A., Atluri, G., Faghmous, J. H., Steinbach, M., Banerjee, A., Ganguly, A., ... & Kumar, V.: Theory-guided data science: A new paradigm for scientific discovery from data, IEEE Transactions on knowledge and data engineering, 29(10), 2318-2331, 2017.

Keating, B. A., Carberry, P. S., Hammer, G. L., Probert, M. E., Robertson, M. J., Holzworth, D., ... & Smith, C. J.: An overview of APSIM, a model designed for farming systems simulation, European journal of agronomy, 18(3-4), 267-288, 2003.

Khandelwal, A., Xu, S., Li, X., Jia, X., Stienbach, M., Duffy, C., ... & Kumar, V., Physics guided machine learning methods for hydrology, arXiv preprint arXiv:2012.02854, 2020.

Kim, T., Jin, Z., Smith, T., Liu, L., Yang, Y., Yang, Y., ... & Zhou, W.: Quantifying nitrogen loss hotspots and mitigation potential for individual fields in the US Corn Belt with a metamodeling approach, Environmental Research Letters, 2021.

Kraft, B., Jung, M., Körner, M., Koirala, S., & Reichstein, M.: Towards hybrid modeling of the global hydrological cycle, Hydrology and Earth System Sciences Discussions, 1-40, 2021.

Meyer, D., Nagler, T., & Hogan, R. J.: Copula-based synthetic data augmentation for machine-learning emulators. Geoscientific Model Development, 14(8), 5205-5215, 2021.

Miller, L. T. , Griffis, T. J., Erickson, M. D., Turner, P. A., Deventer, M. J., Chen, Z., Yu, Z., Venterea, R.T., Baker, J. M., and Frie, A. L.: Response of nitrous oxide emissions to future changes in precipitation and individual rain events, Journal of Environmental Quality, In review, 2021

670   Miller, L. T., Assessing Agricultural Nitrous Oxide Emissions and Hot Moments Using Mesocosm Simulations, (Master

671   Thesis, University of Minnesota) Retrieved from the University of Minnesota Digital Conservancy,

672   https://hdl.handle.net/11299/219276, 2021

673   Necpálová, M., Anex, R. P., Fienen, M. N., Del Grosso, S. J., Castellano, M. J., Sawyer, J. E., ... & Barker, D. W.:

674   Understanding the DayCent model: Calibration, sensitivity, and identifiability through inverse modeling, Environmental

675   Modelling & Software, 66, 110-130, 2015.

676   Oord, A. V. D., Dieleman, S., Zen, H., Simonyan, K., Vinyals, O., Graves, A., ... & Kavukcuoglu, K.: Wavenet: A generative

677   model for raw audio, arXiv preprint arXiv:1609.03499, 2016.

678   Pachauri, R. K., Allen, M. R., Barros, V. R., Broome, J., Cramer, W., Christ, R., ... & van Ypserle, J. P.: Climate change 2014:

679   synthesis report. Contribution of Working Groups I, II and III to the fifth assessment report of the Intergovernmental Panel on

680   Climate Change (p. 151). Ipcc, 2014.

681   Read, J. S., Jia, X., Willard, J., Appling, A. P., Zwart, J. A., Oliver, S. K., ... & Kumar, V.: Process-guided deep learning

682   predictions of lake water temperature, Water Resources Research, 55(11), 9173-9190, 2019.

683   Peng, B., Guan, K., Tang, J., Ainsworth, E. A., Asseng, S., Bernacchi, C. J., ... & Zhou, W.: Towards a multiscale crop

684   modelling framework for climate change adaptation assessment, Nature plants, 6(4), 338-348, 2020.

685   Reichstein, M., Camps-Valls, G., Stevens, B., Jung, M., Denzler, J., & Carvalhais, N.: Deep learning and process understanding

686   for data-driven Earth system science. Nature, 566(7743), 195-204, 2019.

687   Robertson, M., BenDor, T. K., Lave, R., Riggsbee, A., Ruhl, J. B., & Doyle, M.: Stacking ecosystem services, Frontiers in

688   Ecology and the Environment, 12(3), 186-193, 2014.

689   Rohe, L., Apelt, B., Vogel, H. J., Well, R., Wu, G. M., & Schlüter, S.: Denitrification in soil as a function of oxygen availability

690   at the microscale, Biogeosciences, 18(3), 1185-1201, 2021.

691   Saha, D., Basso, B., & Robertson, G. P.: Machine learning improves predictions of agricultural nitrous oxide (N_2O) emissions

692   from intensively managed cropping systems, Environmental Research Letters, 16(2), 024004, 2021.

693   Solazzo, E., Crippa, M., Guizzardi, D., Muntean, M., Choulga, M., & Janssens-Maenhout, G.: Uncertainties in the Emissions

694   Database for Global Atmospheric Research (EDGAR) emission inventory of greenhouse gases, Atmospheric Chemistry and

695   Physics, 21(7), 5655-5683, 2021.

696   Solazzo, E., Crippa, M., Guizzardi, D., Muntean, M., Choulga, M., & Janssens-Maenhout, G.: Uncertainties in the Emissions

697   Database for Global Atmospheric Research (EDGAR) emission inventory of greenhouse gases, Atmospheric Chemistry and

698   Physics, 21(7), 5655-5683, 2021.

699   Syakila, A., & Kroeze, C.: The global nitrous oxide budget revisited, Greenhouse gas measurement and management, 1(1),

700   17-26, 2011.

701   Thompson, R. L., Lassaletta, L., Patra, P. K., Wilson, C., Wells, K. C., Gressent, A., ... & Canadell, J. G.: Acceleration of

702   global N_2O emissions seen from two decades of atmospheric inversion, Nature Climate Change, 9(12), 993-998, 2019.

Thornley, J. H., & France, J.: Mathematical models in agriculture: quantitative methods for the plant, animal and ecological sciences, Cabi, 2007.

Tian, H., Xu, R., Canadell, J. G., Thompson, R. L., Winiwarter, W., Suntharalingam, P., ... & Yao, Y.: A comprehensive quantification of global nitrous oxide sources and sinks, Nature, 586(7828), 248-256, 2020.

Venterea, R. T., Maharjan, B., & Dolan, M. S.: Fertilizer source and tillage effects on yield-scaled nitrous oxide emissions in a corn cropping system. Journal of Environmental Quality, 40(5), 1521-1531, 2011.

Wagner-Riddle, C., Congreves, K. A., Abalos, D., Berg, A. A., Brown, S. E., Ambadan, J. T., ... & Tenuta, M.: Globally important nitrous oxide emissions from croplands induced by freeze–thaw cycles, Nature Geoscience, 10(4), 279-283, 2017.

Willard, J., Jia, X., Xu, S., Steinbach, M., & Kumar, V.: Integrating Scientific Knowledge with Machine Learning for Engineering and Environmental Systems, arXiv preprint arXiv:2003.04919, 2020.

Yang, Y., Liu, L., Zhou, W., Guan, K., Kim, T., Tang, J., Peng, B., Zhu, P., Grant, R. F., Griffis, T. J., Jin, Z.: Distinct driving mechanisms of non-growing season N2O emissions call for spatial-specific mitigation strategies in the US Midwest. One Earth. Submitted, 2022.

Zhang, Y., & Niu, H.: The development of the DNDC plant growth sub-model and the application of DNDC in agriculture: a review, Agriculture, Ecosystems & Environment, 230, 271-282, 2016.

Zhang, Y., Li, C., Zhou, X., & Moore III, B.: A simulation model linking crop growth and soil biogeochemistry for sustainable agriculture, Ecological modelling, 151(1), 75-108, 2002.
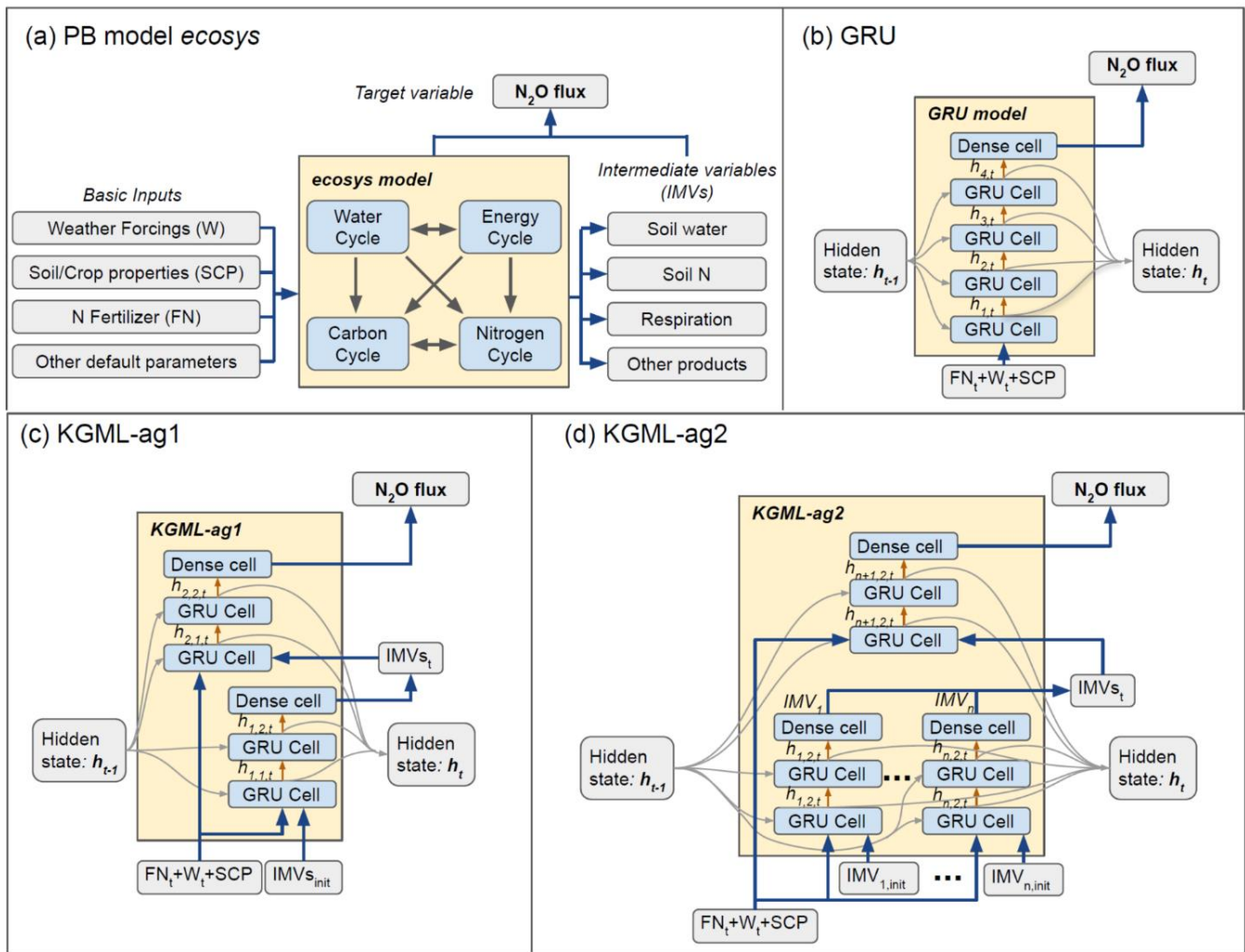
Figure 1: The model structuress. a) The *ecosys* model; b) Gated recurrent unit (GRU) model; c) KGML-ag1 model with a hierarchical structure; d) KGML-ag2 model with a hierarchical structure with separated GRU modules for IMV predictions. Specifically, in our KGML model design, weather forcings (W) include temperature (TMAX, TDIF), precipitation (PRECN), radiation (RADN), humidity (HMAX and HDIF) and wind speed (WIND); soil/crop properties (SCP) include bulk density (TBKDS), sand content (TCSAND), silt content (TCSILT), pH (TPH), cation exchange capacity (TCEC), soil organic carbon (TSOC), planting day of the year (PDOY) and crop type (CROPT); IMVs include CO_2 flux, soil NO_3^- concentration, soil NH_4^+ concentration, and soil volumetric water content (VWC).

731
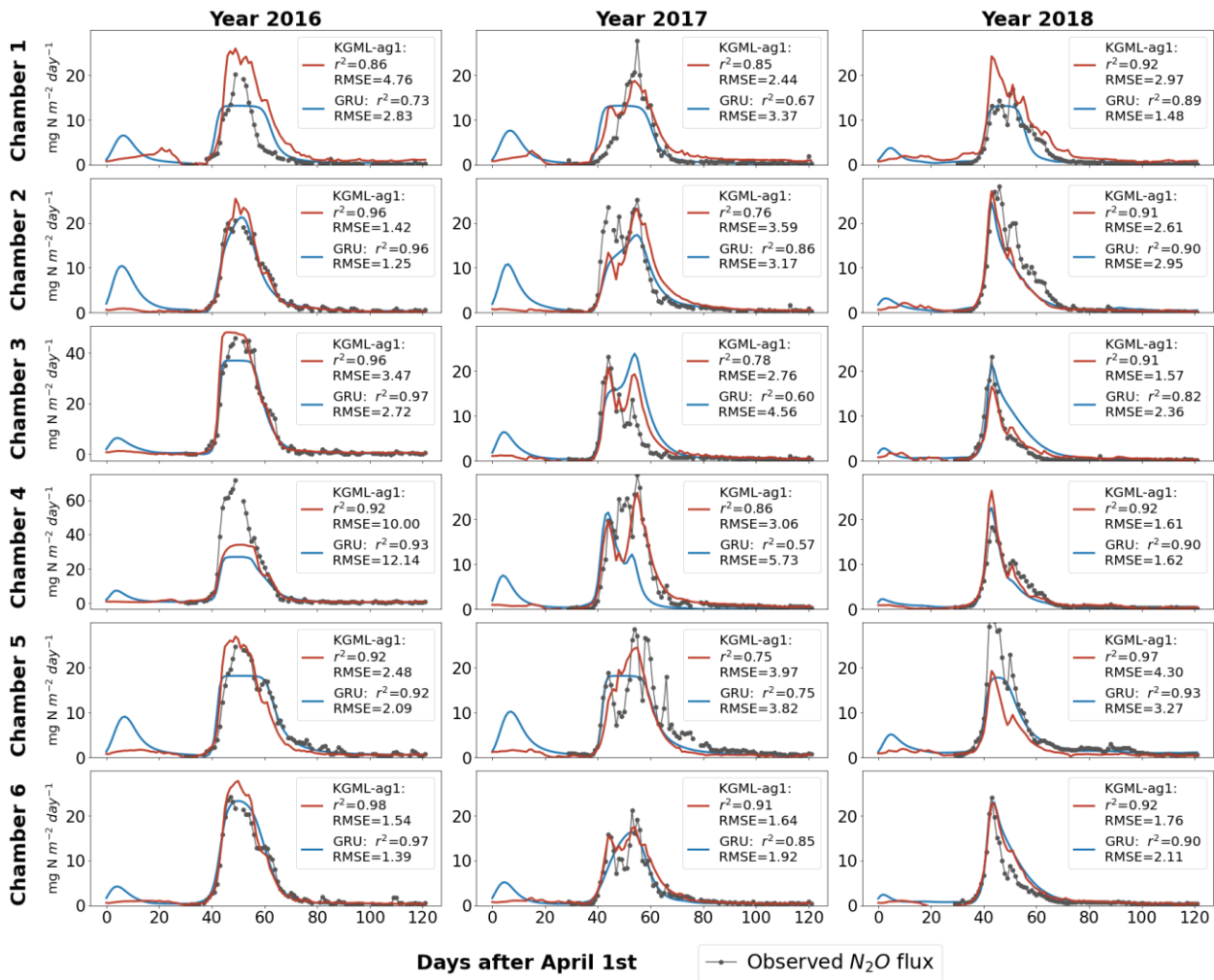
732 **Figure 2: N₂O flux time series comparisons among pure non-pretrained GRU predictions (blue line), KGML-ag1 predictions (red**
733 **line) and observations (black line-dot) from cross-validation. The N₂O flux unit is mg N m⁻² day⁻¹.**

734
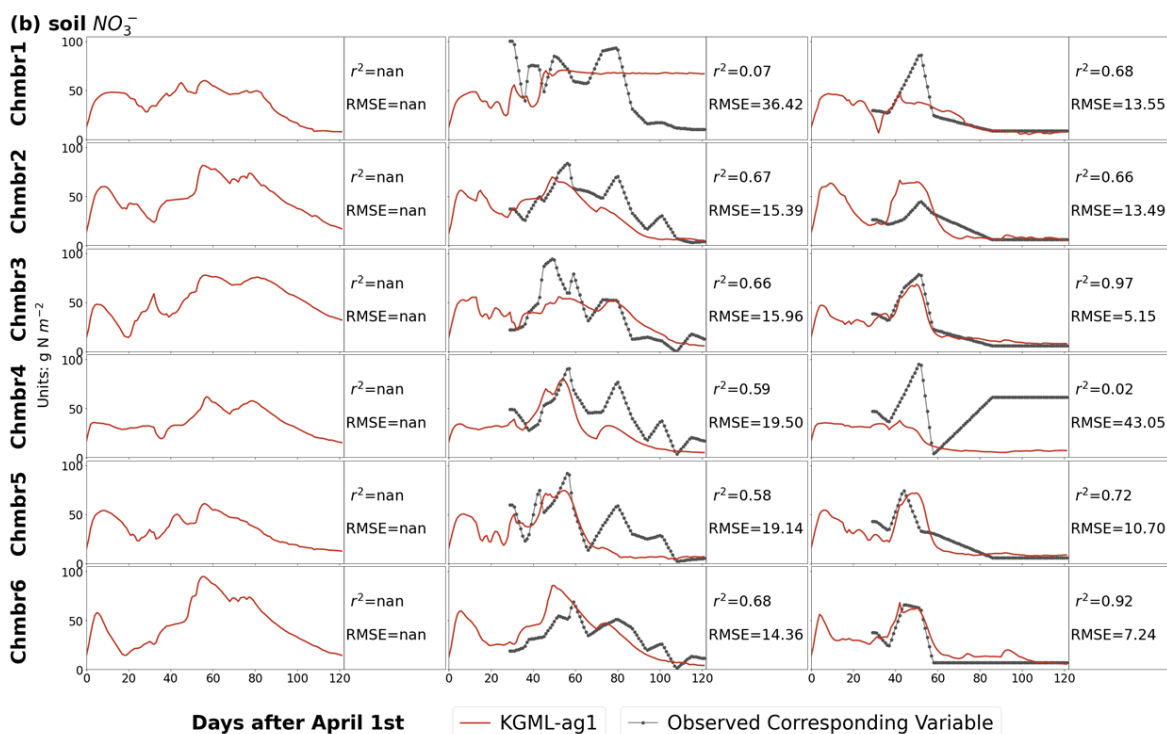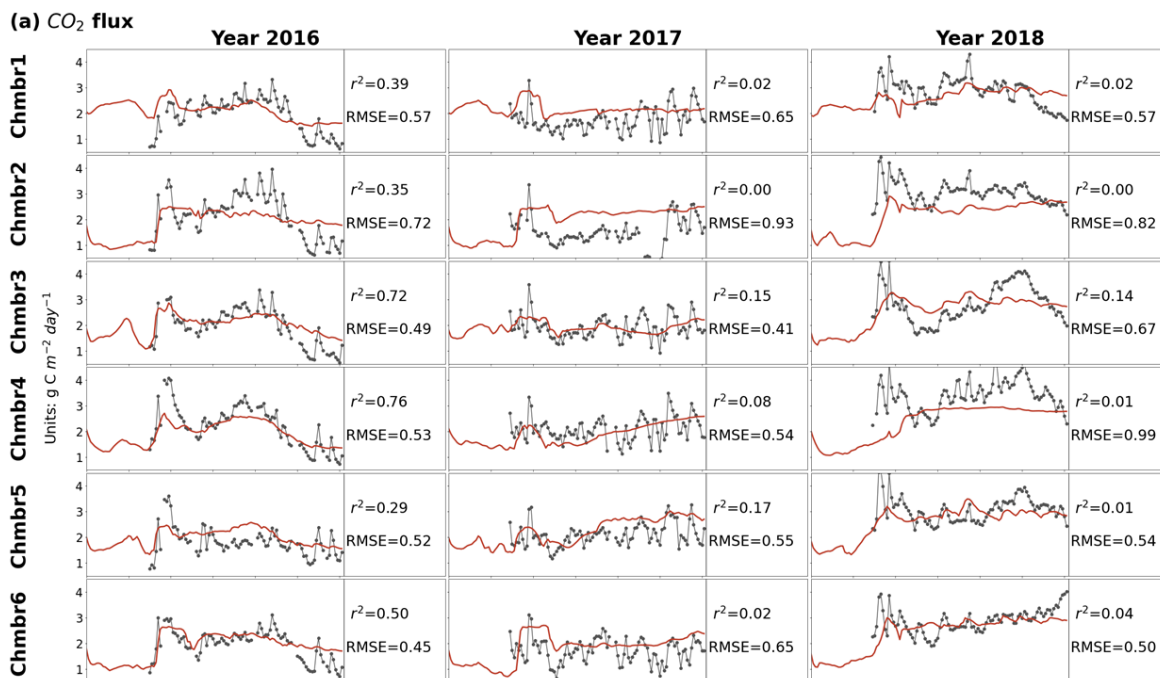
Figure 3: IMVs prediction from KGML-ag1. The black-dot line represents observations and the red line represents the results from KGML-ag1. Chmb is the abbreviation for chamber. r^2 and RMSE are calculated and present in each year and chamber. The CO_2 flux and soil NO_3^- concentration units are g C m^{-2} day^{-1} and g N m^{-2}, respectively.

739
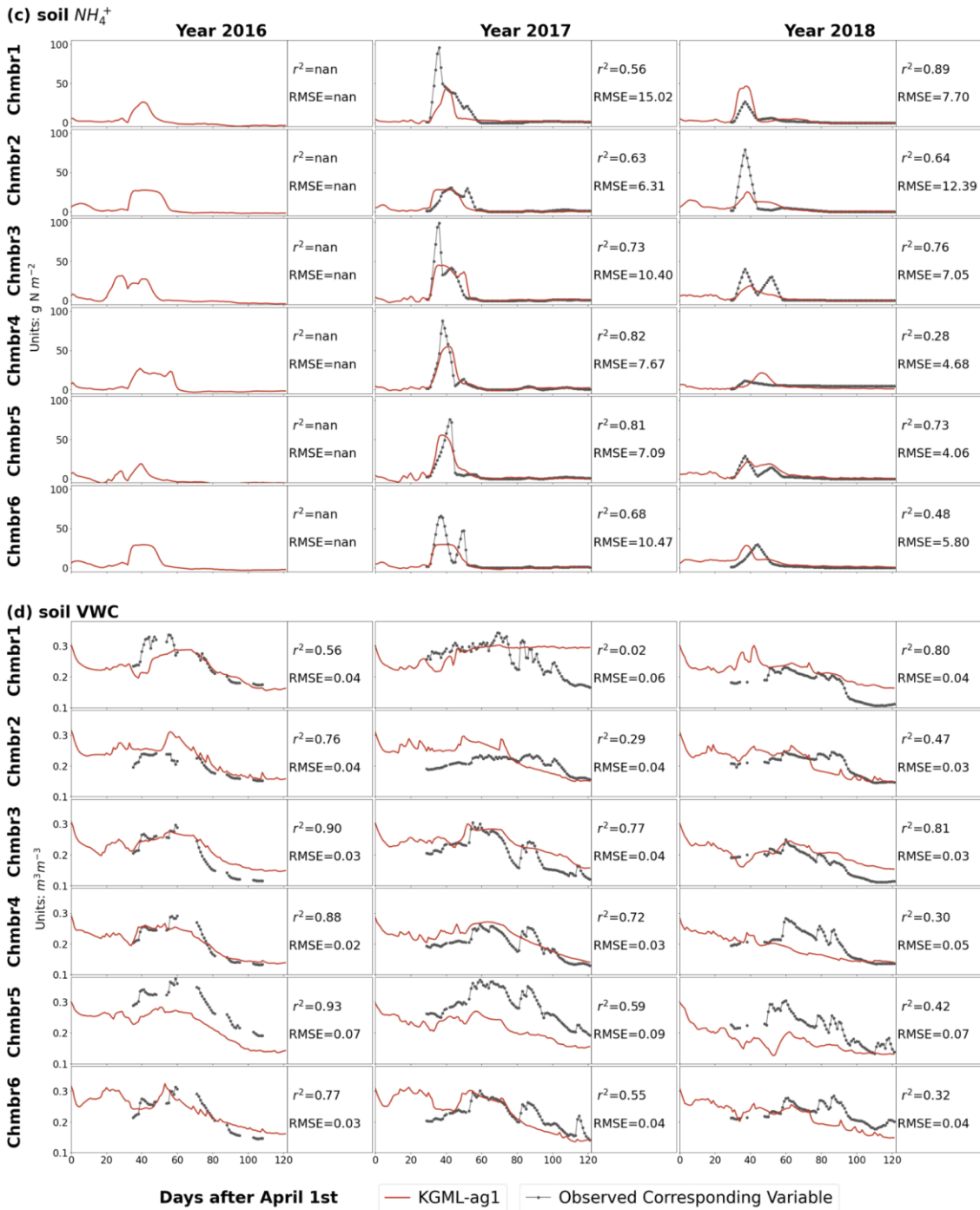
Figure 3 Contd.: IMVs prediction from KGML-ag1. The black-dot line represents observations and the red line represents the results from KGML-ag1. Chmb is the abbreviation for chamber. r^2 and RMSE are calculated and present in each year and chamber. The soil NH_4^+ concentration and soil VWC units are g N m^{-2} and m^3 m^{-3}, respectively.

740
741
742
743

744

745

746
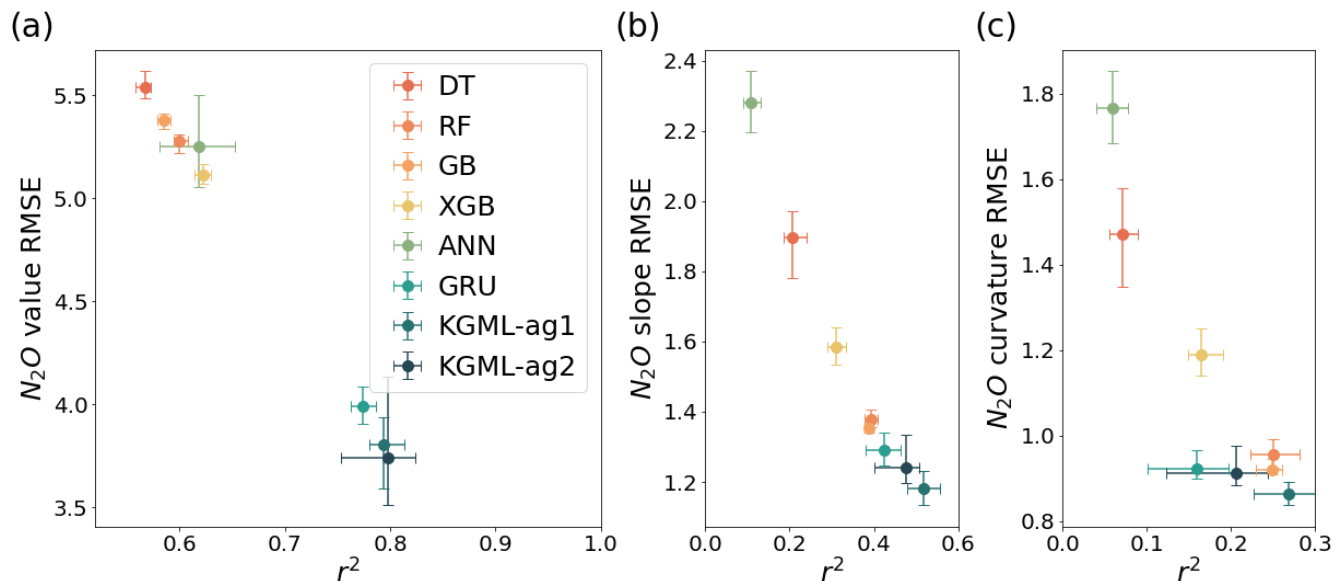
Figure 4: The comparisons of overall prediction accuracy for N_2O value (a), 1st order gradient (slope, b) and 2nd order gradient (curvature, c) between four tree-based ML models (DT, RF, GB and XGB), two deep learning models (ANN and GRU) and KGML-ag models. Different color symbols represent the different models. The x- and y-error bars are coming from the maximum and minimum scores of ensemble experiments. The dot represents the mean score of the ensemble experiments.

751
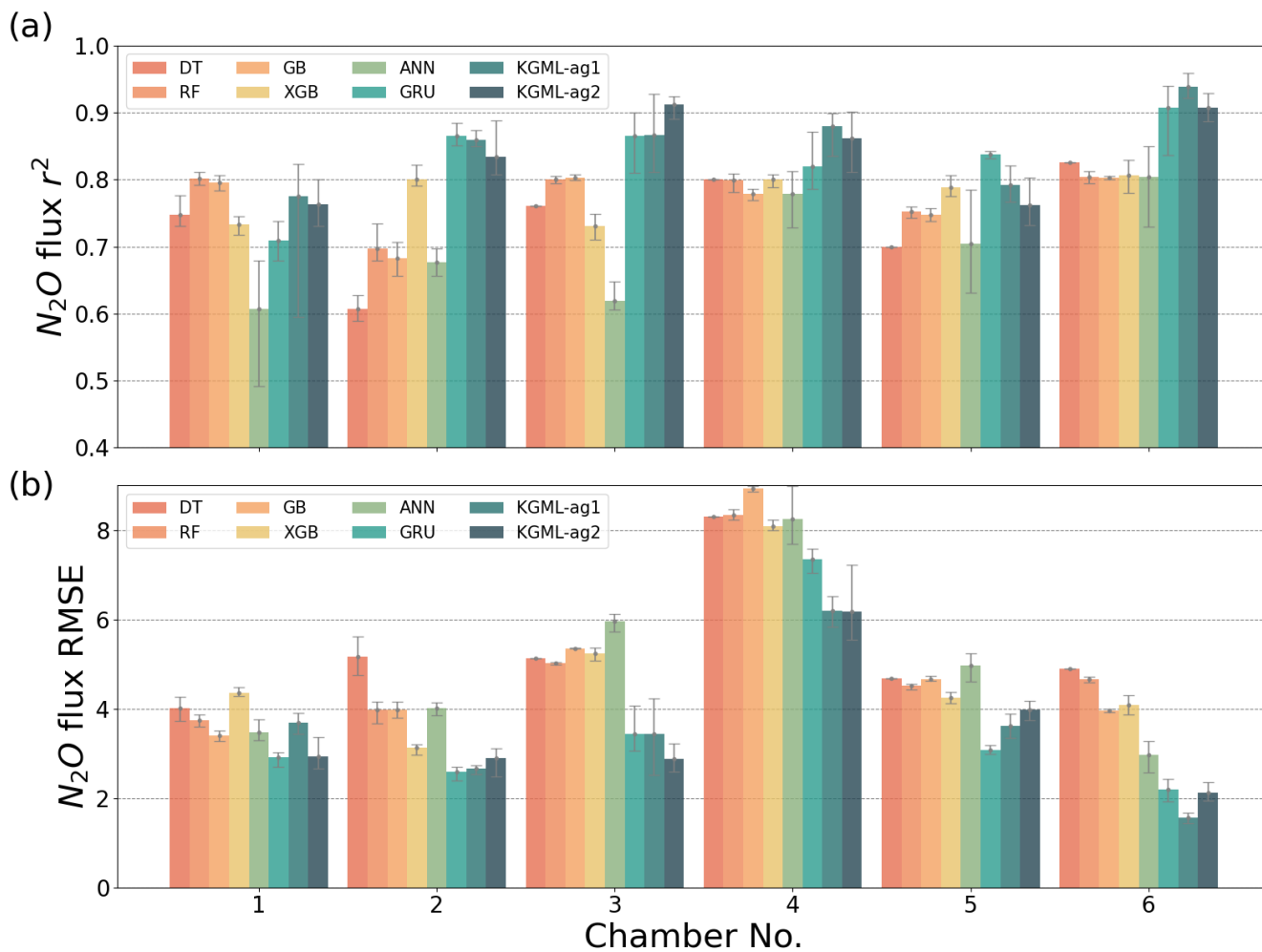
Figure 5: The comparisons of N$_2$O flux prediction accuracy r^2 (a) and (b) RMSE, between four tree-based ML models (DT, RF, GB and XGB), two deep learning models (ANN and GRU) and KGML-ag models in 6 chambers. The gray error bars are coming from the maximum and minimum scores of ensemble experiments.

Table 1: Pretrain results for different model and IMV combinations using *ecosys* synthetic data.

No.	Pretrain Model	Input Feature N	N_2O r^2	RMSE	CO_2 r^2	NRMSE	NO_3^- r^2	NRMSE	NH_4^+ r^2	NRMSE	VWC r^2	NRMSE
1	GRU+76IMVs	76 IMVs+FN+7Ws+8SCP	0.98	0.54	--[a]	--	--	--	--	--	--	--
2	GRU+IMVcb1	4 IMVs+FN+7Ws+8SCP	0.92	1.15	--	--	--	--	--	--	--	--
3	GRU+IMVcb2	3 IMVs+FN+7Ws+8SCP	0.90	1.26	--	--	--	--	--	--	--	--
4	GRU	FN+7Ws+8SCP	0.89	1.37	--	--	--	--	--	--	--	--
5	KGML-ag1+IMVcb1_ini	FN+7Ws+8SCP+4IMV_ini	0.90	1.24	0.91	0.06	0.95	0.03	0.98	0.03	0.95	0.04
6	KGML-ag1+IMVcb2_ini	FN+7Ws+8SCP+3IMV_ini	0.90	1.26	--	--	0.94	0.03	0.97	0.03	0.95	0.04
7	KGML-ag2+IMVcb1_ini	FN+7Ws+8SCP+4IMV_ini	0.90	1.27	0.92	0.05	0.95	0.02	0.98	0.03	0.96	0.04
8	KGML-ag2+IMVcb2_ini	FN+7Ws+8SCP+3IMV_ini	0.91	1.19	--	--	0.95	0.00	0.99	0.02	0.95	0.04

[a]The empty slot indicates that the model does not predict that variable.

Table 2: Prediction accuracy comparisons between non-pretrained GRU model and KGML-ag1.

	No.	N_2O, KGML-ag1 minus GRU All time[b]	Day 30-80	Day 40-65	Day 45-60	N_2O 1st order gradient, KGML-ag1 minus GRU All time	Day 30-80	Day 40-65	Day 45-60	N_2O 2nd order gradient, KGML-ag1 minus GRU All time	Day 30-80	Day 40-65	Day 45-60
Δr^2 [a]	All data	0.03[c]	0.04	0.07	0.10	0.07	0.07	0.07	0.15	0.08	0.08	0.09	0.11
	Chamber1	0.07	0.10	0.20	0.13	0.18	0.18	0.19	0.14	0.08	0.09	0.09	0.02
	Chamber2	-0.04	-0.05	-0.07	-0.05	0.08	0.09	0.09	0.16	0.20	0.20	0.20	0.23
	Chamber3	0.06	0.06	0.08	0.06	0.04	0.04	0.04	0.13	-0.01	-0.01	-0.01	0.07
	Chamber4	0.06	0.08	0.12	0.07	0.05	0.05	0.05	0.14	0.07	0.07	0.08	0.12
	Chamber5	-0.05	-0.06	-0.07	-0.03	0.09	0.09	0.10	0.16	0.13	0.13	0.15	0.11
	Chamber6	0.03	0.04	0.08	0.17	0.14	0.14	0.15	0.22	0.12	0.13	0.14	0.23
$\Delta RMSE$ [a]	All data	-0.41	-0.56	-0.84	-1.19	-0.07	-0.10	-0.14	-0.20	-0.03	-0.05	-0.07	-0.08
	Chamber1	0.80	1.06	1.21	1.70	0.00	0.00	-0.02	0.00	0.05	0.07	0.10	0.18
	Chamber2	0.08	0.11	0.07	-0.04	-0.10	-0.13	-0.18	-0.14	-0.10	-0.14	-0.19	-0.22
	Chamber3	-0.71	-0.96	-1.30	-2.09	0.03	0.04	0.07	-0.25	0.09	0.13	0.17	0.08
	Chamber4	-1.68	-2.27	-3.09	-3.81	-0.11	-0.15	-0.21	-0.26	-0.05	-0.07	-0.09	-0.16
	Chamber5	0.53	0.69	0.86	0.99	-0.10	-0.14	-0.20	-0.23	-0.09	-0.12	-0.18	-0.14
	Chamber6	-0.20	-0.27	-0.37	-0.61	-0.14	-0.20	-0.29	-0.33	-0.07	-0.10	-0.15	-0.19

[a]The difference of r^2 (Δr^2), and difference of RMSE ($\Delta RMSE$, units are mg N m^{-2} day^{-1}, mg N m^{-2} day^{-2}, mg N m^{-2} day^{-3} for N_2O value, 1st order gradient and 2nd order gradient, respectively) were calculated by values from KGML-ag1 minus values from GRU.

[b]Results from different time windows of different chambers during the period of April 1st-July31st (Days1-122) were detected.

[c]Blue cells mean KGML-ag1 outperforms GRU, while yellow cells mean the opposite.

767 **Table 3: Experiments for measuring GRU and KGML-ag models performance, and influence of pretraining process, training data**
768 **augmentation and IMV initial values.**

No.	Retrain Model	Experiment	N$_2$O r^2	N$_2$O RMSE	N$_2$O 1st order gradient r^2	N$_2$O 1st order gradient RMSE	N$_2$O 2nd order gradient r^2	N$_2$O 2nd order gradient RMSE	CO$_2$ r^2	CO$_2$ NRMSE	NO$_3^-$ r^2	NO$_3^-$ NRMSE	NH$_4^+$ r^2	NH$_4^+$ NRMSE	VWC r^2	VWC NRMSE
1	GRU, baseline[a]	No Pretrain	0.78	4.00	0.45	1.27	0.20	0.90	--[b]	--	--	--	--	--	--	--
2	GRU	Pretrain	0.80	3.77	0.57	1.12	0.34	0.82	--	--	--	--	--	--	--	--
3	KGML-ag1+ IMVcb1_ini	Original setting	0.81	3.60	0.51	1.20	0.28	0.87	0.37	0.14	0.39	0.21	0.60	0.09	0.33	0.18
4	KGML-ag1+ IMVcb2_ini	Original setting	0.80	3.71	0.49	1.22	0.21	0.91	--	--	0.37	0.22	0.53	0.10	0.33	0.19
5	KGML-ag2+ IMVcb1_ini	Original setting	0.79	3.77	0.48	1.23	0.22	0.90	0.74	0.09	0.46	0.18	0.66	0.08	0.84	0.08
6	KGML-ag2+ IMVcb2_ini	Original setting	0.78	3.91	0.47	1.24	0.20	0.91	--	--	0.49	0.18	0.69	0.08	0.84	0.08
7	KGML-ag1+ IMVcb1_ini	No augmentation	0.80	3.73	0.49	1.22	0.22	0.90	0.38	0.14	0.38	0.21	0.61	0.09	0.37	0.17
8	KGML-ag1+ IMVcb2_ini	No augmentation	0.77	4.04	0.41	1.31	0.13	0.95	--	--	0.38	0.21	0.53	0.10	0.35	0.18
9	KGML-ag2+ IMVcb1_ini	No augmentation	0.76	4.06	0.45	1.27	0.16	0.95	0.69	0.10	0.21	0.25	0.60	0.09	0.80	0.09
10	KGML-ag2+ IMVcb2_ini	No augmentation	0.74	4.27	0.48	1.23	0.21	0.90	--	--	0.40	0.21	0.60	0.09	0.81	0.09
11	KGML-ag1+ IMVcb1_ini	Zero initial values	0.48	6.27	0.26	1.49	0.08	1.00	0.19	0.16	0.25	0.25	0.47	0.12	0.14	0.25
12	KGML-ag1+ IMVcb2_ini	Zero initial values	0.49	5.94	0.31	1.41	0.13	0.95	--	--	0.31	0.25	0.38	0.13	0.24	0.25
13	KGML-ag2+ IMVcb1_ini	Zero initial values	0.48	6.05	0.12	1.66	0.01	1.09	0.58	0.12	0.34	0.25	0.21	0.13	0.56	0.31
14	KGML-ag2+ IMVcb2_ini	Zero initial values	0.39	6.60	0.15	1.59	0.04	1.01	--	--	0.16	0.27	0.27	0.12	0.53	0.31

769 [a]Gray region includes the experiments with original simulation settings as described in Sec. 2 and dark gray refers to the baseline GRU
770 simulation; Blue region includes the experiments without data augmentation during the finetuning process; And yellow region includes the
771 experiments of replacing original IMV initial values with zeros.
772 [b]The empty slot indicates that the model does not predict that variable.
773